

**An experimental comparison of proportional-integral, sliding mode, and robust adaptive control for piezo-actuated nanopositioning stages**

Guo-Ying Gu and Li-Min Zhu

Citation: [Review of Scientific Instruments](#) **85**, 055112 (2014); doi: 10.1063/1.4876596

View online: <http://dx.doi.org/10.1063/1.4876596>

View Table of Contents: <http://scitation.aip.org/content/aip/journal/rsi/85/5?ver=pdfcov>

Published by the [AIP Publishing](#)

---

**Articles you may be interested in**

[Robust synchronization of chaotic systems subject to parameter uncertainties](#)

Chaos **19**, 033128 (2009); 10.1063/1.3212940

[Synchronization of a class of chaotic systems with fully unknown parameters using adaptive sliding mode approach](#)

Chaos **18**, 043112 (2008); 10.1063/1.3013601

[Synchronization of two different chaotic systems using novel adaptive fuzzy sliding mode control](#)

Chaos **18**, 033133 (2008); 10.1063/1.2980046

[Stabilization of an underactuated mechanical system by sliding mode control](#)

AIP Conf. Proc. **1019**, 80 (2008); 10.1063/1.2953058

[Robust Second Order Sliding mode Observer for the Estimation of the Vehicle States](#)

AIP Conf. Proc. **1019**, 27 (2008); 10.1063/1.2952992

---

**GRANVILLE-PHILLIPS®**

ADVANCED VACUUM MEASUREMENT SOLUTIONS

Vacuum Gauges:

Convectron®, Micro-Ion®, Stabil-Ion®,  
Cold Cathode

Mass Spectrometers:

Vacuum Quality Monitors



[www.brooks.com](http://www.brooks.com)

Introducing the First  
Cold Cathode Gauge  
worthy of the  
Granville-Phillips name!

- Unsurpassed Accuracy
- Predictive & Easy Maintenance



# An experimental comparison of proportional-integral, sliding mode, and robust adaptive control for piezo-actuated nan positioning stages

Guo-Ying Gu<sup>a)</sup> and Li-Min Zhu

State Key Laboratory of Mechanical System and Vibration, Shanghai Jiao Tong University, Shanghai 200240, China

(Received 23 January 2014; accepted 3 May 2014; published online 23 May 2014)

This paper presents a comparative study of the proportional-integral (PI) control, sliding mode control (SMC), and robust adaptive control (RAC) for applications to piezo-actuated nan positioning stages without the inverse hysteresis construction. For a fair comparison, the control parameters of the SMC and RAC are selected on the basis of the well-tuned parameters of the PI controller under same desired trajectories and sampling frequencies. The comparative results show that the RAC improves the tracking performance by 17 and 37 times than the PI controller in terms of the maximum tracking error  $e_m$  and the root mean tracking error  $e_{rms}$ , respectively, while the RAC improves the tracking performance by 7 and 9 times than the SMC in terms of  $e_m$  and  $e_{rms}$ , respectively. © 2014 AIP Publishing LLC. [<http://dx.doi.org/10.1063/1.4876596>]

## I. INTRODUCTION

Recently, piezo-actuated stages receive more and more attentions in a variety of nan positioning applications.<sup>1,2</sup> The key elements of piezo-actuated stages are piezoceramic actuators (PCAs), which have excellent advantages of large output force, high resolution, and fast response time. However, the PCAs have the inherent hysteresis nonlinearity, severely degrading the accuracy of the piezo-actuated stages. In practice, the maximum error caused by the hysteresis nonlinearity can be more than 15% of the travel range if the PCAs operate in the open-loop condition.<sup>3,4</sup>

To remedy the hysteresis nonlinearity, many interesting works have been reported in the literature. It has been shown that a mathematical model could facilitate the controller design for hysteresis compensation.<sup>5</sup> In this sense, the foremost task is to develop a hysteresis model to characterize the hysteresis nonlinearity. Then, a feedforward inverse compensator can be designed to cancel the hysteresis nonlinearity.<sup>6-9</sup> Considering the fact that the inversion-based approach lacks of robustness, feedback control is usually applied with the feedforward control for piezo-actuated stages.<sup>3,10-12</sup> However, the hysteresis models are usually very complicated, which lead to the great calculation costs of the inverse constructions, even impossible to construct an analytical inverse. Instead of constructing the inverse hysteresis models, some attempts have been made to directly design feedback control laws for hysteresis compensation, such as proportional-integral (PI) control,<sup>13</sup> sliding model control (SMC),<sup>14-16</sup> and robust adaptive control (RAC).<sup>4,17-19</sup> Despite significant body of work on the development of feedback control strategies without the inverse hysteresis construction, the experimental comparative study of them on a piezo-actuated stage is rare until now.

In this paper, we present an experimental comparison of three feedback control strategies, i.e., PI control, SMC, and RAC for piezo-actuated nan positioning stages. The three

control strategies are designed with the hysteresis decomposition method without constructing the inverse hysteresis model. The SMC and RAC are presented to compare with the PI control in this work because the PI controller is a basic structure of the designed SMC and RAC. In experiments, the control parameters of the three controllers are all selected on the basis of the well-tuned parameters of the PI controller, and the measurements are taken for each control method under the same sampling frequencies and desired trajectories. Comparative experimental results show that the RAC achieves superior tracking performance for nan positioning applications.

The contribution of this work is twofold. (i) With the hysteresis decomposition method, a real-time experimental comparison of the PI control, SMC, and RAC for piezo-actuated stages is first presented in this work although the three control strategies are known in the literature. (ii) In practice, there is no rules to tune the parameters of the SMC and RAC. In this work, the presented SMC and RAC are based on the PI control. The well-tuned control parameters of the PI controller can be directly used in SMC and RAC, which provides a tuning method for the practical applications of SMC and RAC.

The remainder of this paper is organized as follows. Section II states the description and dynamic modeling of the piezo-actuated stage. In Sec. III, the developed controllers are presented, and comparative experimental tests are conducted in Sec. IV. Finally, Sec. V concludes this paper.

## II. DESCRIPTION OF THE PIEZO-ACTUATED STAGE

### A. System setup

A schematic structure of the piezo-actuated stage to be controlled in this work is shown in Fig. 1. The stage<sup>20</sup> is composed of a flexure-hinge-based mechanism driven by two PCAs for decoupled XY parallel motion, where the end-effector is connected to the base by four independent kinematic limbs and two types of compound flexure modules are serially connected to provide two degree-of-freedom motion. The voltage amplifier with a fixed gain of 10 provides

<sup>a)</sup>Electronic mail: [guguaying@sjtu.edu.cn](mailto:guguaying@sjtu.edu.cn).

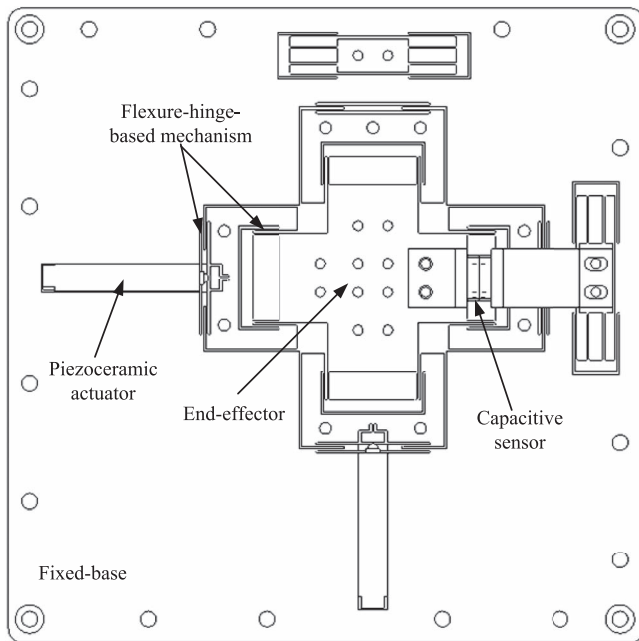


FIG. 1. Schematic structure of a flexure-hinge-based mechanism.

voltage input in the range 0–100 V for the PCA of each axis. The resultant motion produced by the platform is within a workspace of  $40\ \mu\text{m} \times 40\ \mu\text{m}$ . This motion is measured by the two-plate capacitive sensors and fed into an electronic position servo-control module. The output of this module is in the range of 0–10 V with the sensitivity of  $10\ \mu\text{m}/\text{V}$ .

To control the stage, a dSPACE-DS1103 rapid prototyping control board equipped with 16-bit analog to digital converters (ADCs) and 16-bit digital to analog converters (DACs) is utilized to implement real-time control laws in the MATLAB/Simulink environment. Due to the characteristics of the dSPACE, the control voltage of the designed controllers for the voltage amplifier is normalized with respect to 0–10 V range, while the real-time captured position of the capacitive sensors is normalized with respect to 0–100  $\mu\text{m}$ . In this work, the sampling frequency of this system is set to 20 kHz. The whole experimental platform is depicted in Fig. 2. It is worthy of mentioning that the designed stage is well decoupled, thus the two-axis motions can be treated independently. Therefore, two single-input-single-output controllers can be designed for  $x$ -axis and  $y$ -axis of the stage, respectively. Considering the comparative objective of different control approaches, only the treatment of  $x$ -axis motion tracking is presented in this paper.

## B. Hysteresis decomposition

As addressed in Sec. I, the challenge for control of the piezo-actuated stage lies in the fact that the hysteresis nonlinearity of the PCA severely degrades the tracking performance. In this work, we try to find a method suitable for fusion with available control approaches to mitigate the effect of hysteresis without the inverse hysteresis construction. For this purpose, we adopt an approximate linear relationship to capture the overall slope of the hysteresis curve and leave the

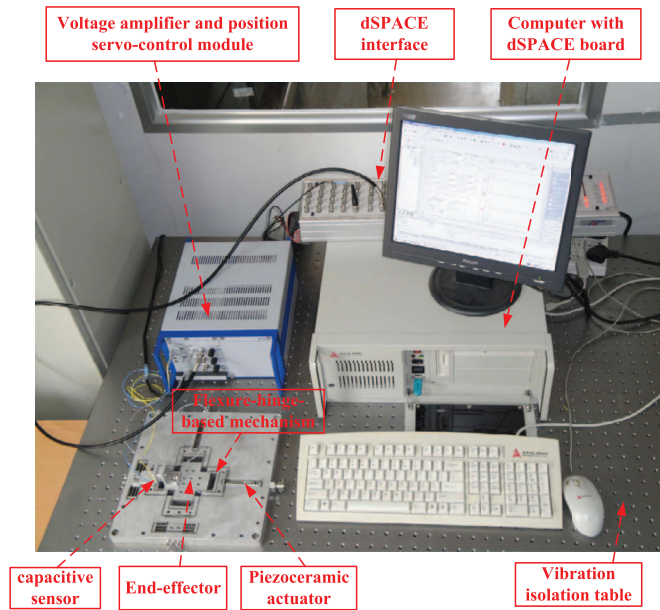


FIG. 2. A picture of the experimental setup.

unknown nonlinear term as a bounded disturbance to be well compensated by the feedback laws.

In general, the hysteresis nonlinearity can be denoted as the following operator

$$w(t) = H[v](t), \quad (1)$$

where  $w(t)$  is the output of hysteresis, usually unmeasurable,  $v(t)$  is the control input given to the PCA. As shown in Fig. 3, the nonlinear hysteresis (1) can be decomposed into a linear part  $K$  and a bounded nonlinear disturbance  $d$ .

Following this decomposition, the solution of the operator (1) can be expressed as

$$w(t) = H(v(t)) = cv(t) + d(v(t)). \quad (2)$$

As an illustration, Fig. 4 shows the linear representation of the nonlinear hysteresis operator  $H[v](t)$  by (2) with the nonlinear bounded disturbance  $d(v(t))$  satisfying  $|d(v(t))| \leq \rho$ . In the following, we will simply write  $d(t)$  to denote  $d(v(t))$ .

## C. Dynamic modeling

The dynamic model of the piezo-actuated nanopositioning stage can be described by two cascaded parts in terms of an input hysteresis nonlinearity and a linear dynamic plant, which is schematically represented by Fig. 5. The block  $\hat{H}[v](t)$  takes care of the hysteresis nonlinearity, which has been addressed in Sec. II B. The block  $G(s)$  is a lumped model

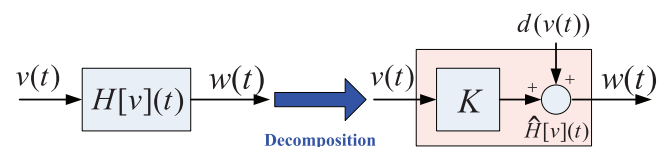


FIG. 3. Decomposition of the hysteresis nonlinearity.

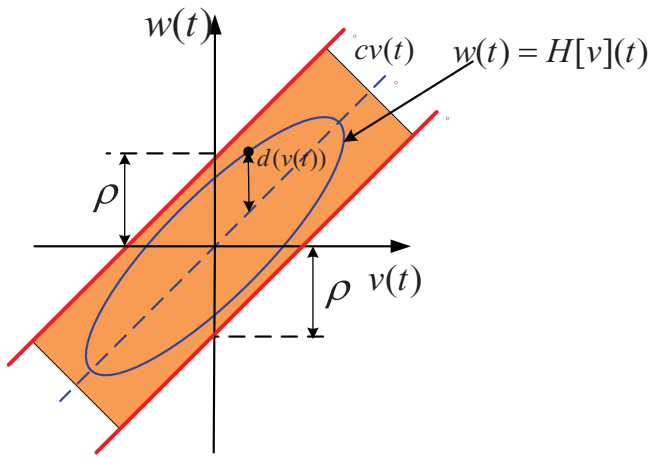


FIG. 4. Schematic representation of the hysteresis operator  $H[v](t)$  with a linear relation to the input signal  $v(t)$  plus a nonlinear bounded term  $d(v(t))$ .

for the plant dynamics by a s-domain transfer function. As addressed in Refs. 4, 21, and 22, the linear dynamic model  $G(s)$  can be represented in the Laplace domain as follows:

$$G(s) = \frac{k\omega_n^2}{(\tau s + 1)(s^2 + 2\zeta\omega_n s + \omega_n^2)}, \quad (3)$$

where  $s$  is the Laplace variable,  $k$ ,  $\tau$ ,  $\zeta$ , and  $\omega$  are system parameters.

*Remark:* It should be noted that the first-order pole of the dynamic model (3) is introduced when the electrical behavior of the voltage amplifier is considered for system modeling of the piezo-actuated nanopositioning stage.<sup>4</sup> The reader may refer to Ref. 4 for the detailed modeling approach and discussions.

To validate the model (3), the dynamic frequency response of the stage is previously conducted using band-limited white noise signals. The low-amplitude control voltage for the stage is restricted within 2 V to avoid distortion from hysteresis as much as possible.<sup>17,23</sup> The experimental bode plot is shown in Fig. 6. Using System Identification Tool of MATLAB, the linear dynamic model (3) is identified as

$$G(s) = \frac{2.352 \times 10^9}{(s + 400)(s^2 + 283.1s + 2.291 \times 10^7)}. \quad (4)$$

For comparison, the frequency response of the identified model (4) is also shown in Fig. 6, which implies that the third-order model well captures the linear dynamics of the stage. Note that the input and output signals of the frequency response are normalized and a constant sensor delay is taken into account. In the following development, we will show that

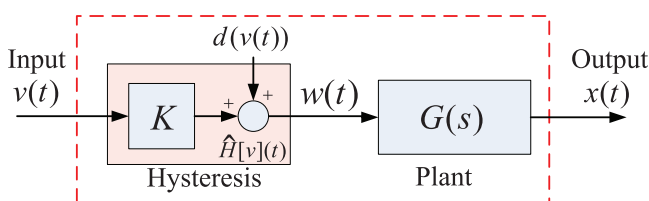


FIG. 5. Block diagram of the dynamic model of the piezo-actuated stage with hysteresis decomposition.

the first-order model can capture the system dynamics within the frequency of interest. Then, we will utilize a reduced first-order model to illustrate the way to fuse the hysteresis model with different control approaches for the comparative study.

To elucidate the first-order model response, an open-loop step test is conducted. To restrict the influences of hysteresis nonlinearity over large displacements and creep nonlinearity over long time periods,<sup>17,23</sup> small-amplitude step response during the first 0.03 s is captured. Figure 7 shows a 0.1-V step response of the piezo-actuated positioning stage which is indicated by the blue solid line. Based on the characteristics of the transient response, the plant dynamics can be well represented by the first-order model response with the transfer function  $104/(s + 400)$ . In Fig. 7, the model simulation response indicated by the red dashed line is compared with the experimental response to verify the effectiveness of the model. In addition, the first-order model response is presented in Fig. 6 for a clear understanding of the following controller design. Therefore, combining (2), the identified dynamic model of the piezo-actuated stage is expressed as

$$\dot{x}(t) + a_0x(t) = b_0(cv(t) + d(t)), \quad (5)$$

where  $a_0 = 400$ ,  $b_0 = 104$ , and  $c = 1$ .

*Remark:* It is worthy of mentioning that the following developed controllers can also be designed for the second-order or third-order system. However, in such a case, much complicated design procedures are required, which will dominate the weights of the presented material. To balance and demonstrate the advantages of the proposed control approach with hysteresis decomposition in practice, the reduced first-order model that captures the system dynamics within the frequencies of interest is used to design the controller as an initial illustration for the piezo-actuated nanopositioning stage.

### III. CONTROLLER DEVELOPMENT

With the hysteresis decomposition method as shown in Fig. 5, PI control, SMC, and RAC will be designed in this section for a piezo-actuated stage (5). Figure 8 shows the control scheme of the closed-loop system. The control objective is to design a control law for  $v(t)$  in (5) to force the plant position  $x(t)$  to follow a specified desired trajectory  $x_d(t)$  in the presence of disturbances.

#### A. PI control

With its three-term functionality covering treatment to both transient and steady-state responses, PI control offers the simplest solution and yet most efficient solution in some applications.<sup>24</sup> It has been widely applied for control of commercial piezo-actuated positioning stages, for instance, in Refs. 13 and 25 and reference therein.

A conventional PI controller can be implemented as follows:

$$v(t) = K_p \left[ e(t) + \frac{1}{T_i} \int_0^t e(\tau) d\tau \right], \quad (6)$$

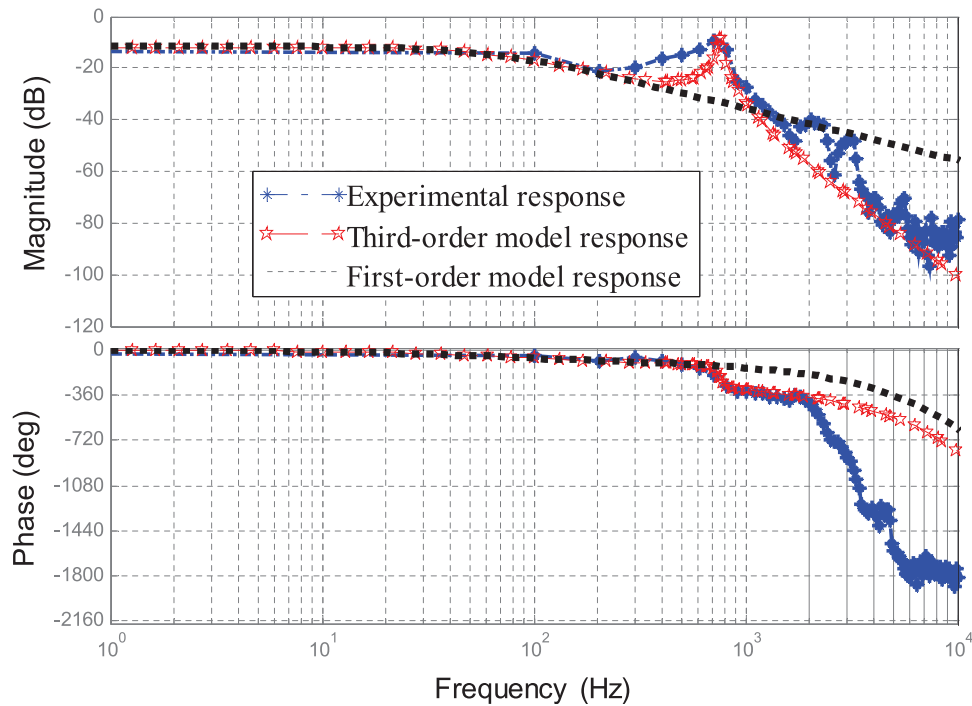


FIG. 6. Frequency response of the piezo-actuated stage.

where  $e(t) = x_d(t) - x(t)$  is the tracking error,  $v(t)$  is the control output,  $K_p$  and  $T_i$  are the proportional gain and integral time, respectively.

**B. SMC**

The sliding surface is defined as

$$s(t) = \left(\frac{d}{dt} + \lambda\right) \left(\int_0^t \tilde{x}(r) dr\right) = \tilde{x}(t) + \lambda \int_0^t \tilde{x}(r) dr, \quad (7)$$

where  $\tilde{x}(t) = x(t) - x_d(t)$  represents the tracking error,  $\lambda > 0$  is the designed parameter such that the sliding mode on  $s = 0$  is stable. It can be seen that (7) is equivalent to (6).

The control action of traditional sliding mode is discontinuous in nature due to the switching control at the reaching

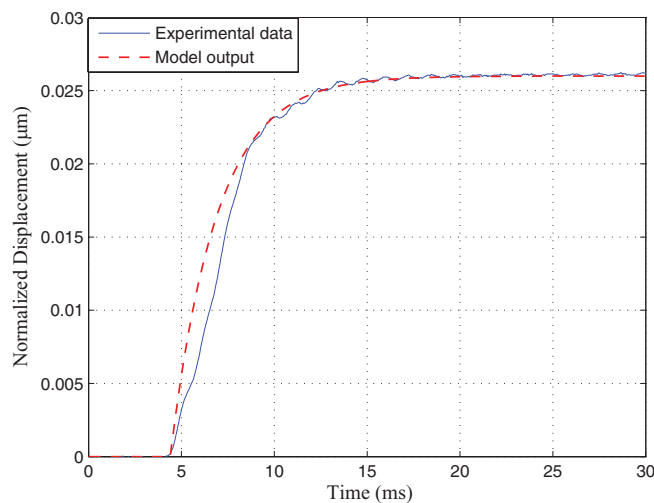


FIG. 7. Step response of the piezo-actuated stage.

mode.<sup>14–16,26</sup> It may lead to the chattering phenomenon, thus triggers the high frequency un-modeled dynamics. In order to avoid the chattering phenomena, a tuning error is introduced

$$s_\epsilon = s - \epsilon \text{sat}(s/\epsilon), \quad (8)$$

where  $\epsilon$  is an arbitrary positive constant and  $\text{sat}(\cdot)$  is the standard saturation function defined as

$$\text{sat}(z) = \begin{cases} 1, & \text{for } z \geq 1 \\ z, & \text{for } -1 < z < 1 \\ -1, & \text{for } z \leq -1. \end{cases} \quad (9)$$

For convenience in presenting the designed control laws, the following definitions are made:

$$\theta = \frac{a_0}{b_0c}, \quad \phi = \frac{1}{b_0c}, \quad (10)$$

where  $a_0$  and  $b_0$  are the system parameters in (5). It is necessary to note that the following practical assumption is required to develop the controllers.

*Assumption:* The extent of parameter uncertainties in (5) satisfies

$$\theta \in \Omega_\theta \triangleq \{\theta : \theta_{min} \leq \theta \leq \theta_{max}\}, \quad (11)$$

$$\phi \in \Omega_\phi \triangleq \{\phi : \phi_{min} \leq \phi \leq \phi_{max}\}, \quad (12)$$

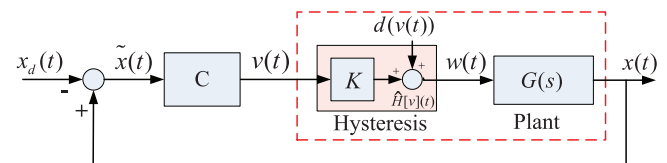


FIG. 8. Block of the closed-loop system (block  $C$  represents the developed controller).

where  $\theta_{min}$ ,  $\theta_{max}$ ,  $\phi_{min}$ , and  $\phi_{max}$  are some known real numbers.

With the above definitions, the control law of the SMC is developed as follows:

$$v(t) = -k_d s + \phi(\dot{x}_d(t) - \lambda \tilde{x}(t)) + \theta x(t) - k^* \text{sat}(s/\epsilon), \quad (13)$$

where  $\epsilon$  is an arbitrary positive constant,  $k_d > 0$ , and  $k^*$  is control gain, satisfying  $k^* \geq \frac{\rho}{c}$ .

### C. RAC

In the above SMC law (13), the system parameters (5) are required as known constant. However, in real physical systems, due to the modeling uncertainties the control law may introduce an infinite gain in the feedback loop. To overcome this drawback, it is desirable to estimate the parameters on-line to handle the parameters uncertainties of the system (5) for trajectory tracking.<sup>4,17-19</sup> For this purpose, an adaptive control law shall be integrated with the SMC into a RAC strategy that can mitigate both the parameter uncertainties and uncertain nonlinearities.

In presenting the RAC laws, the following definitions are given:

$$\tilde{\theta} = \hat{\theta} - \theta, \quad \tilde{\phi} = \hat{\phi} - \phi, \quad (14)$$

where  $\hat{\theta}$  is an estimate of  $\theta$ , and  $\hat{\phi}$  is an estimate of  $\phi$ .

To estimate the system parameters, a projection operator  $\text{proj}(\hat{z}, -y)$  is utilized, which is formulated as

$$\text{proj}(\hat{z}, -y) = \begin{cases} 0, & \text{if } \hat{z} = z_{max} \text{ and } y < 0 \\ -y, & \text{otherwise} \\ 0, & \text{if } \hat{z} = z_{min} \text{ and } y > 0. \end{cases} \quad (15)$$

The control laws of the RAC are then developed as follows:

$$v(t) = -k_d s + \hat{\phi} u_{fd}(t) + \hat{\theta} x(t) - k^* \text{sat}(s/\epsilon), \quad (16)$$

$$u_{fd}(t) = \dot{x}_d(t) - \lambda \tilde{x}(t), \quad (17)$$

$$\hat{\phi} = \text{proj}(\hat{\phi}, -\eta \dot{x}_d s \epsilon), \quad (18)$$

$$\hat{\theta} = \text{proj}(\hat{\theta}, -\gamma x s \epsilon), \quad (19)$$

where  $\epsilon$  is an arbitrary positive constant,  $k_d > 0$ , and  $k^*$  is control gain, satisfying  $k^* \geq \frac{\rho}{c_{min}}$ . In addition, the parameters  $\eta$  and  $\gamma$  are positive constants determining the rates of adaptations.

## IV. EXPERIMENTAL RESULTS

To compare the controller performance, each control strategy will be applied to the custom-built stage as shown in Fig. 2. The developed control laws are implemented into S-function files in MATLAB using C language for real-time control purpose at a sampling frequency of 20 kHz.

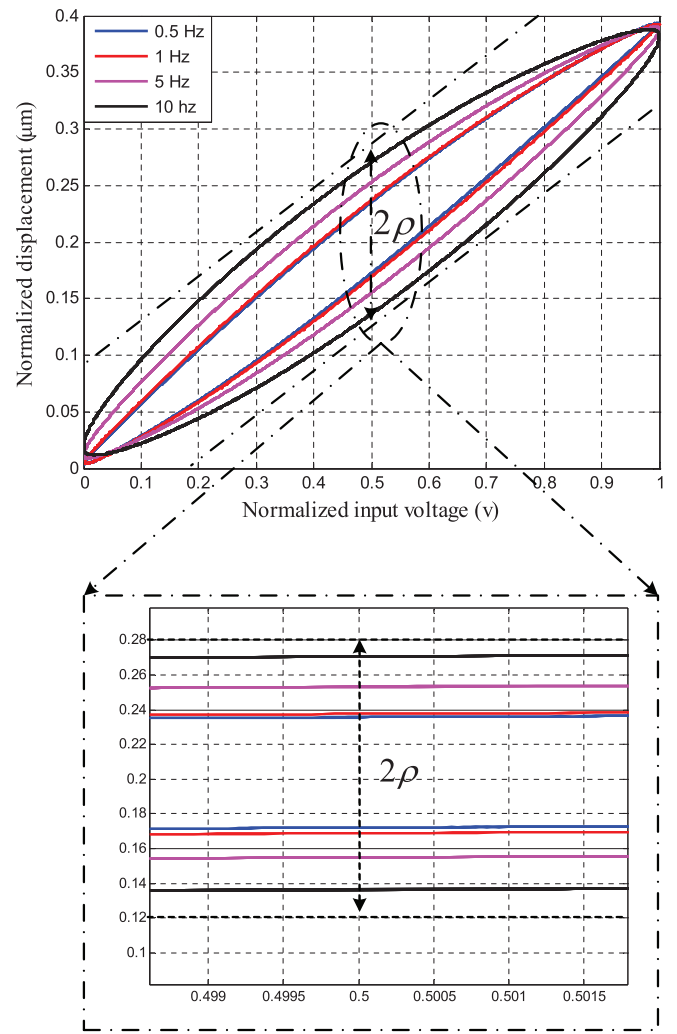


FIG. 9. Normalized hysteresis loops of the piezo-actuated stage.

### A. Open loop tests

Open loop tests of the piezo-actuated stage are first conducted to obtain the bounded term  $\rho$  through the experimental data. Figure 9 shows the normalized major-loop hysteresis curves captured by the dSPACE system under different frequencies of the sinusoidal control input. We observe that the piezo-actuated stage has severe hysteresis nonlinearity in the open-loop strategy, where the maximum hysteresis height with respect to the full displacement range of the piezo-actuated stage is about 40%. It cannot work well for high-precision motion tracking applications without the developed control approaches applied on it. This work adopts an approximate linear relationship to capture the overall slope of the hysteresis curve and leaves the unknown nonlinear term as a bounded disturbance to be compensated by the developed controllers. Before implementation of the control laws, it is necessary to obtain the bounded term  $\rho$  with the prior open-loop experimental data. According to the hysteresis decomposition method addressed in Sec. II B, the value of  $\rho$  is determined as  $\rho = 0.08$  from the external hysteresis loop as shown in Fig. 9.

## B. Comparative study

In this work, the parameters of the PI controller are properly pre-tuned using the trial and error method. The parameters are experimentally chosen as  $K_p = 1$  and  $T_i = 0.0018$ . It should be mentioned that the parameters of the PI sliding surface in SMC are chosen the same as the ones of the PI controller. The difference between PI control and SMC lies on existence of the robust part in the SMC laws (13). In addition,  $k^*$  is chosen as 0.2 and the other designed parameters of the SMC law are selected as  $k_d = 1$ ,  $\lambda = 1/0.0018$ , and  $\epsilon = 0.025$ . Furthermore, comparing with the SMC law (13), the RAC laws (16) have the same structure and differ only in the projection operator based adaptive laws. In order to have a fair comparison between the SMC and RAC, the designed control parameters of the sliding mode part are selected as  $k_d = 1$ ,  $\lambda = 1/0.0018$ ,  $k^* = 0.2$ , and  $\epsilon = 0.025$ , which are the same in the PI control and SMC laws. For the adaptive part, the parameters  $\eta$  and  $\gamma$  determining the rates of adaptations are chosen as  $\eta = 5$  and  $\gamma = 500$ . Moreover, the initial values for the system parameters are set to  $\hat{\theta}(0) = 400/104$  and  $\hat{\phi}(0) = 1/104$ , which are the nominal values used in the SMC law. The bounds of the parameter variations are estimated as  $\theta_{min} = 0.5$ ,  $\theta_{max} = 5$ ,  $\phi_{min} = 0.001$ , and  $\phi_{max} = 0.03$ . Therefore, the designed parameters of RAC are the same with the ones of SMC, and the only difference from the SMC is the adaptive law to estimate the plant parameters on-line.

For the desired trajectory shown in Fig. 10, Fig. 11 shows the tracking errors with the PI control, SMC, and RAC. For quantified comparison, the maximum tracking error  $e_m$  and the root mean tracking error  $e_{rms}$  are depicted in Fig. 12. It can be seen that the RAC improves the tracking performance by 17 and 37 times than the PI control in terms of  $e_m$  and  $e_{rms}$ , respectively, while the RAC improves the tracking performance by 7 and 9 times than the SMC in terms of  $e_m$  and  $e_{rms}$ , respectively. Furthermore, Fig. 13 shows the relationship between actual and desired position. It can be obtained that the maximum resulting hysteresis errors are about 10%, 3%, and 0.5% of the full displacement range with the PI control, SMC, and

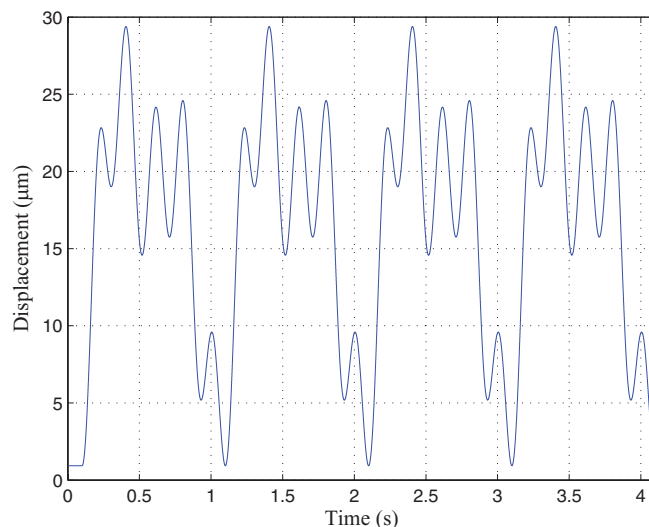


FIG. 10. Desired trajectory.

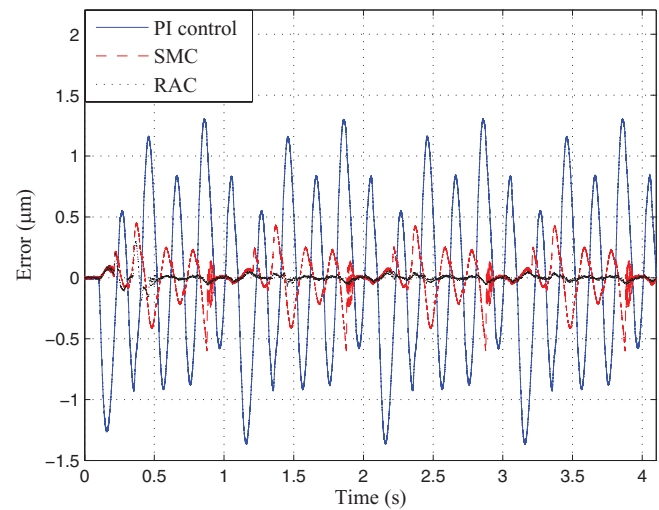


FIG. 11. Comparisons of tracking errors with PI control (indicated by the solid blue line), SMC (indicated by the dashed red line), and RAC (indicated by the dotted black line).

RAC, respectively, which also demonstrates the outperforming performances of the RAC.

## C. Discussion

The experimental results show that the PI control has the worst tracking performance. However, the PI control is yet the simplest approach to be implemented. Significantly, better results are achieved by using the SMC and RAC with the robust control action. The limitation of the SMC is the use of the fixed nominal system parameters. With the introduction of the adaptive control action, the system parameters can be estimated on-line to handle the plant uncertainties. Thus, the RAC achieves best tracking performance verified by experimental results. To further elucidate the characteristics of different control approaches, comparative experimental tests are conducted under desired trajectories with different frequencies. Table I lists the tracking performances of the three

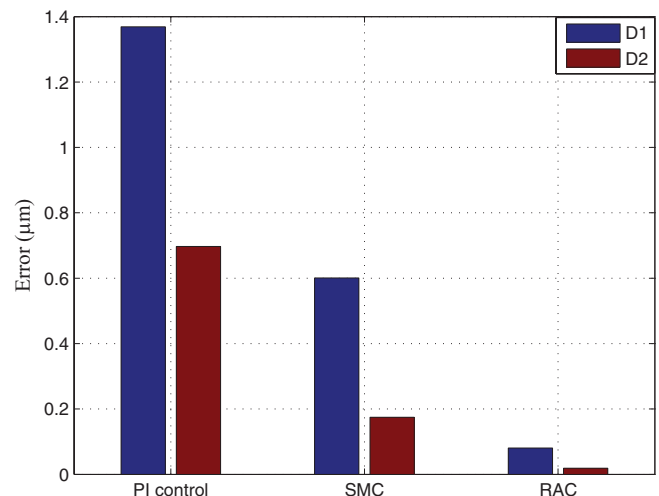


FIG. 12. Comparison of the tracking performances of different controllers (D1- $e_m$ ; D2- $e_{rms}$ ).

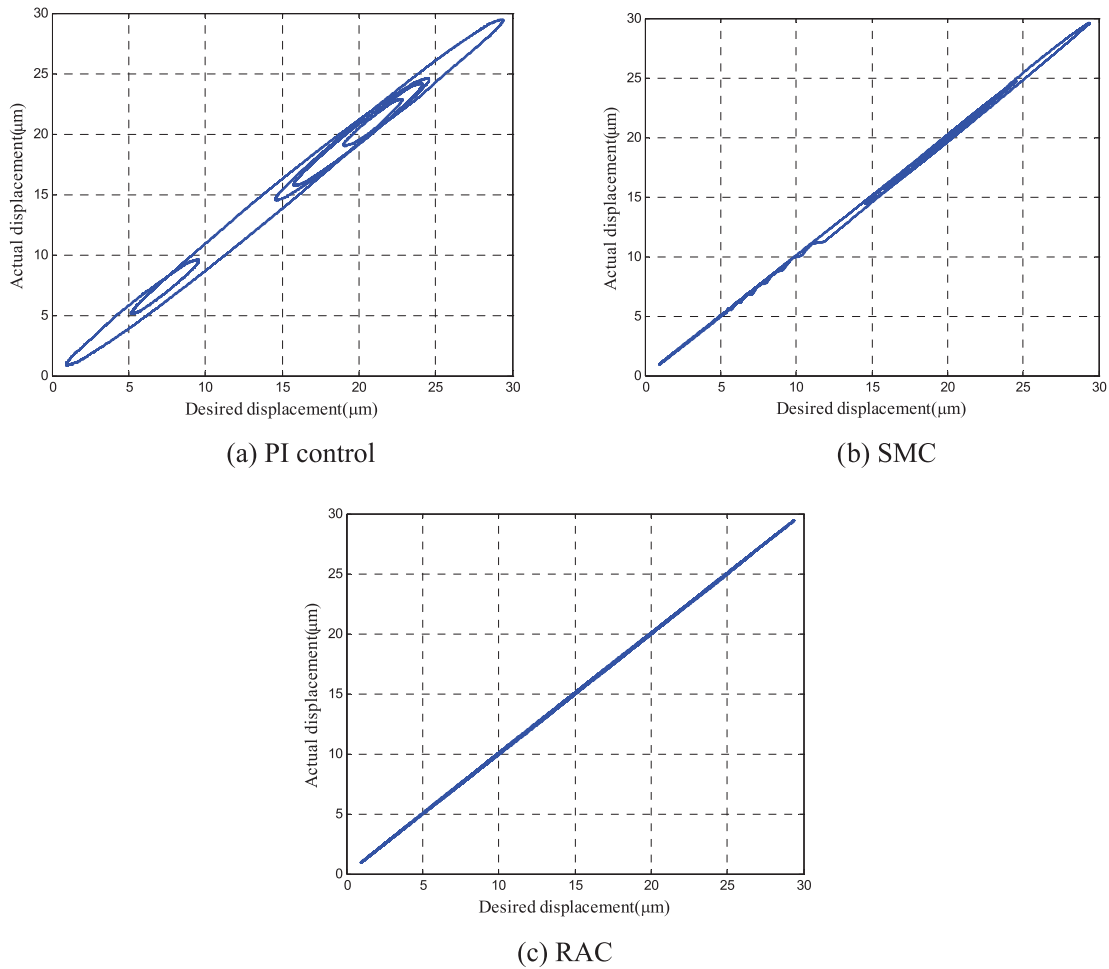


FIG. 13. Actual versus desired position with different controllers.

controllers with  $e_m$  and  $e_{rms}$ . It can be observed that with increasing input frequencies, the tracking errors increase as well since the high-order dynamics of the system is not considered in this work, which will be recognized as a future work. Overall, the comparative studies demonstrate that the RAC sufficiently improves the tracking precision and outperforms the SMC and PI control for nanopositioning applications.

TABLE I. Tracking performances of PI control, SMC, and RAC with the 20  $\mu\text{m}$  p-p displacement range under different trajectory frequencies.

Frequency (Hz)	Controller	$e_m$ (nm)	$e_{rms}$ (nm)
0.5	PI control	176.7	120.6
	SMC	78.2	34.3
	RAC	19.0	4.4
1	PI control	345.3	238.3
	SMC	147.2	68.0
	RAC	23.4	7.2
5	PI control	1773.7	1227.1
	SMC	653.7	325.9
	RAC	43.4	18.7
10	PI control	3627.3	2464.1
	SMC	1248.3	640.2
	RAC	86.1	40.5

## V. CONCLUSION

A detailed comparison of three feedback control approaches with the PI control, SMC, and RAC has been presented for applications to piezo-actuated nanopositioning stages. The control approaches considered in this paper are designed without constructing the inverse hysteresis model. In experiments, the designed control parameters of different controllers are all based on the designed parameters of the PI controller, and the measurements are taken for each control approach under the same sampling frequencies and desired trajectories. Comparative experimental results show that the RAC achieves superior tracking performance than the SMC and PI control for nanopositioning applications.

## ACKNOWLEDGMENTS

This work was in part supported by National Natural Science Foundation of China under Grant No. 91023047, Specialized Research Fund for the Doctoral Program of Higher Education under Grant No. 20130073110037, and Open Research Foundation of State Key Laboratory of Digital Manufacturing Equipment and Technology in Huazhong University of Science and Technology under Grant No. DMETKF2014004.

- <sup>1</sup>Y. K. Yong, S. O. R. Moheimani, B. J. Kenton, and K. K. Leang, "Invited review article: High-speed flexure-guided nanopositioning: Mechanical design and control issues," *Rev. Sci. Instrum.* **83**, 121101 (2012).
- <sup>2</sup>A. J. Fleming, "Dual-stage vertical feedback for high-speed scanning probe microscopy," *IEEE Trans. Control Syst. Technol.* **19**, 156–165 (2011).
- <sup>3</sup>P. Ge and M. Jouaneh, "Tracking control of a piezoceramic actuator," *IEEE Trans. Control Syst. Technol.* **4**, 209–216 (1996).
- <sup>4</sup>G. Y. Gu, L. M. Zhu, C. Y. Su, and H. Ding, "Motion control of piezoelectric positioning stages: modeling, controller design and experimental evaluation," *IEEE/ASME Trans. Mechatron.* **18**, 1459–1471 (2013).
- <sup>5</sup>K. Kuhnen and P. Krejci, "Compensation of complex hysteresis and creep effects in piezoelectrically actuated systems: A new Preisach modeling approach," *IEEE Trans. Autom. Control* **54**, 537–550 (2009).
- <sup>6</sup>X. L. Zhao and Y. H. Tan, "Modeling hysteresis and its inverse model using neural networks based on expanded input space method," *IEEE Trans. Control Syst. Technol.* **16**, 484–490 (2008).
- <sup>7</sup>M. A. Janaideh, S. Rakheja, and C. Y. Su, "An analytical generalized Prandtl–Ishlinskii model inversion for hysteresis compensation in micropositioning control," *IEEE/ASME Trans. Mechatron.* **16**, 734–744 (2011).
- <sup>8</sup>G. Y. Gu, M. J. Yang, and L. M. Zhu, "Real-time inverse hysteresis compensation of piezoelectric actuators with a modified Prandtl–Ishlinskii model," *Rev. Sci. Instrum.* **83**, 065106 (2012).
- <sup>9</sup>W. Li, X. Chen, and Z. Li, "Inverse compensation for hysteresis in piezoelectric actuator using an asymmetric rate-dependent model," *Rev. Sci. Instrum.* **84**, 115003 (2013).
- <sup>10</sup>C. H. Ru and L. N. Sun, "Improving positioning accuracy of piezoelectric actuators by feedforward hysteresis compensation based on a new mathematical model," *Rev. Sci. Instrum.* **76**, 095111 (2005).
- <sup>11</sup>M. Rakotondrabe, C. Cleve, and P. Lutz, "Robust feedforward-feedback control of a nonlinear and oscillating 2-DOF piezocantilever," *IEEE Trans. Autom. Sci. Eng.* **8**, 506–519 (2011).
- <sup>12</sup>Y. Shan and K. K. Leang, "Dual-stage repetitive control with Prandtl–Ishlinskii hysteresis inversion for piezo-based nanopositioning," *Mechatronics* **22**, 271–281 (2012).
- <sup>13</sup>S. Devasia, E. Eleftheriou, and S. O. R. Moheimani, "A survey of control issues in nanopositioning," *IEEE Trans. Control Syst. Technol.* **15**, 802–823 (2007).
- <sup>14</sup>H. C. Liaw, B. Shirinzadeh, and J. Smith, "Enhanced sliding mode motion tracking control of piezoelectric actuators," *Sens. Actuators, A* **138**, 194–202 (2007).
- <sup>15</sup>J. C. Shen, W. Y. Jywe, and C. H. Liu, "Sliding-mode control of a three-degrees-of-freedom nanopositioner," *Asian J. Control* **10**, 267–276 (2008).
- <sup>16</sup>J. Y. Peng and X. B. Chen, "Integrated PID-based sliding mode state estimation and control for piezoelectric actuators," *IEEE/ASME Trans. Mechatron.* **19**, 88–99 (2014).
- <sup>17</sup>J. H. Zhong and B. Yao, "Adaptive robust precision motion control of a piezoelectric positioning stage," *IEEE Trans. Control Syst. Technol.* **16**, 1039–1046 (2008).
- <sup>18</sup>S. Bashash and N. Jalili, "Robust adaptive control of coupled parallel piezoflexural nanopositioning stages," *IEEE/ASME Trans. Mechatron.* **14**, 11–20 (2009).
- <sup>19</sup>Y. Li and Q. Xu, "Adaptive sliding mode control with perturbation estimation and PID sliding surface for motion tracking of a piezo-driven micromanipulator," *IEEE Trans. Control Syst. Technol.* **18**, 798–810 (2010).
- <sup>20</sup>L. J. Lai, G. Y. Gu, and L. M. Zhu, "Design and control of a decoupled two degree of freedom translational parallel micro-positioning stage," *Rev. Sci. Instrum.* **83**, 045105 (2012).
- <sup>21</sup>H. Adriaens, W. L. de Koning, and R. Banning, "Modeling piezoelectric actuators," *IEEE/ASME Trans. Mechatron.* **5**, 331–341 (2000).
- <sup>22</sup>Y. S. Gao, D. W. Zhang, and C. W. Yu, "Dynamic modeling of a novel workpiece table for active surface grinding control," *Int. J. Mach. Tools Manuf.* **41**, 609–624 (2001).
- <sup>23</sup>K. K. Leang and S. Devasia, "Feedback-linearized inverse feedforward for creep, hysteresis, and vibration compensation in AFM piezoactuators," *IEEE Trans. Control Syst. Technol.* **15**, 927–935 (2007).
- <sup>24</sup>K. H. Ang, G. Chong, and Y. Li, "PID control system analysis, design, and technology," *IEEE Trans. Control Syst. Technol.* **13**, 559–576 (2005).
- <sup>25</sup>A. J. Fleming, "Nanopositioning system with force feedback for high-performance tracking and vibration control," *IEEE/ASME Trans. Mechatron.* **15**, 433–447 (2010).
- <sup>26</sup>J.-J. E. Slotine and W. Li, *Applied Nonlinear Control* (Prentice-Hall, New Jersey, 1991).